SCIENTIFIC REPORTS

OPEN

SUBJECT AREAS:
ELECTRONIC STRUCTURE
THERMOELECTRICS
TWO-DIMENSIONAL MATERIALS
TOPOLOGICAL INSULATORS

Received
11 September 2014

Accepted
6 January 2015

Published
29 January 2015

Correspondence and requests for materials should be addressed to D.W. (dong913@tsinghua.edu.cn)

Few-quintuple Bi_2Te_3 nanofilms as potential thermoelectric materials

Gang Zhou & Dong Wang

MOE Key Laboratory of Organic OptoElectronics and Molecular Engineering, Department of Chemistry, Tsinghua University, Beijing, 100084, People's Republic of China.

The thermoelectric transport properties of p-type Bi_2Te_3 nanofilms with various quintuple layers (QL) were systematically investigated based on *ab initio* electronic structure calculations and Boltzmann transport equations. Our results demonstrated that p-type few-quintuple Bi_2Te_3 nanofilms could exhibit high thermoelectric performance. It was found out that the 1QL Bi_2Te_3 nanofilm had the highest *ZT* value as compared with other nanofilms, which is mainly attributed to the significant enhancement of the density of states near the edge of the valence band resulting from the strong coupling between the top and bottom electronic states and the quantum confinement effect. The dependence of the thermoelectric transport properties on carrier concentration and temperature was also discussed in detail, which can be useful for searching high-efficiency few-quintuple Bi_2Te_3 thermoelectric nanofilms.

Thermoelectric materials have attracted intense interest due to their potential applications in cooling and power generation[1–5]. The performance of thermoelectric devices depends on the dimensionless figure of merit, *ZT*, which is defined as

$$ZT = \frac{S^2 \sigma T}{\kappa_l + \kappa_e}, \tag{1}$$

where S is the Seebeck coefficient, T is the temperature, σ is the electrical conductivity, κ_l is the lattice thermal conductivity and κ_e is the thermal conductivity of the electronic carriers. To achieve a high *ZT*, it requires maximizing the Seebeck coefficient and electrical conductivity but minimizing the thermal conductivity. In general, the thermal conductivity can be minimized by introducing nanostructures into the thermoelectric materials to increase phonon scattering[6–8], the Seebeck coefficient can be enhanced by quantum confinement effects[9,10], and the electrical conductivity can be improved by adjusting the carrier concentration through doping[11,12], however, the interdependence among these parameters makes the maximization of *ZT* a challenge so far.

Among various thermoelectric materials, Bi_2Te_3 and its solid solutions have been investigated intensely because they possess outstanding thermoelectric properties at room temperature, which is due to the high degeneracy at the edges of their energy bands. The *ZT* value of the Bi_2Te_3-based thermoelectric materials has been improved by many approaches such as the synthesis of nanostructured bulk materials or nanocomposites with a precise control of the size, structure, composition and carrier concentration as well as the deposition of various thin films by melt-spinning, sputtering, evaporation and molecular beam epitaxy[13–16]. Recently, Bi_2Te_3 has been demonstrated as a three-dimensional (3D) topological insulator, which further stimulates a strong research interest in this material[17]. Bulk Bi_2Te_3 crystallizes in a rhombohedral unit cell with the space group D_{3d}^5 ($R\bar{3}m$) and has a layered structure with five atomic layers referred to as a quintuple layer (QL)[18,19]. The interaction between two adjacent QL is of the weak van der Waals type, which allows one to disassemble Bi_2Te_3 crystal into its quintuple building block[20]. The experimental results have shown that the exfoliated quintuples and ultrathin few-quintuple films have a low thermal conductivity, which is favorable to improve the thermoelectric performance[20]. Very recently, an efficient thermoelectric conversion was observed in the atomic monolayer steps of Bi_2Te_3 (n-type) and Sb_2Te_3 (p-type) QL by scanning photoinduced thermoelectric current probe[21]. Theoretically, P. Ghaemi *et al.* have discovered that nanometer-scale Bi_2Te_3 thin film generates a hybridization-induced band gap of the unconventional surface states, which can lead to an increased thermoelectric performance at low temperatures[22]. Recent theoretical researches show that Bi_2Te_3 nanofilms have enhanced thermoelectric properties[18,23]. B. Qiu *et al.* have studied the thermal conductivity of the few-quintuple Bi_2Te_3 nanofilms by using molecular dynamics simulation and have shown that nanoporous Bi_2Te_3 nanofilms display significantly reduced

thermal conductivity as compared to the bulk couterparts[24]. All these results indicate that the few-quintuple Bi_2Te_3 nanofilms can be considered as promising thermoelectric materials.

In this work, we report an effective scheme of combining density functional theory and Boltzmann transport equations to provide a microscopic description of the thermoelectric properties of few-quintuple Bi_2Te_3 nanofilms. Our results demonstrate that p-type few-quintuple Bi_2Te_3 nanofilms can exhibit high thermoelectric performance and thus they can stand as a promising candidate for nanoscale thermoelectric applications.

Computational methods

First-principles calculation. The calculation of the energy band structure has been performed by using the projector augmented wave (PAW) method within the framework of density functional theory as implemented in the Vienna *Ab initio* Simulation Package (VASP)[25–27]. The exchange-correlation function is in the form of the Perdew-Burke-Ernzerh (PBE) with generalized gradient approximation (GGA)[28,29]. The Monkhorst-Pack scheme is adopted for the integration of Brillouin zone with a **k** mesh of 11 × 11 × 11 for the bulk Bi_2Te_3 and a **k** mesh of 11 × 11 × 1 for the Bi_2Te_3 few-quintuple films. In order to investigate the transport properties of the Bi_2Te_3 nanofilms, a denser **k** mesh of 45 × 45 × 1 is used. A cutoff energy of 450 eV is used in the plane wave basis. For the lattice constants one uses experimental value[30], and interlayer separations for Bi_2Te_3 few-quintuple nanofilms are fully relaxed until the magnitude of the force acting on all atoms is less than 0.01 eV/Å and the total energy converges within 0.001 meV. The Bi_2Te_3 nanofilms with various thicknesses are modeled as a slab containing a few quintuples and a vacuum layer, and Fig. 1 shows the models used in this simulation. For the five slabs with different thicknesses considered, a vacuum layer of 28 Å is added. Our tests revealed that this is sufficient for the prevention of spurious interactions between image slabs.

Calculation of the transport properties. In this work, the semi-classical Boltzmann equations with the relaxation time approximation were used to evaluate the thermoelectric transport coefficients[31]. Previous calculations confirmed that it is an effective approach to predict the thermoelectric transport properties of bulk materials and nanosystems[9,32,33]. By solving the Boltzmann transport equations, σ, S and κ_e can be obtained as[9,34]

$$\sigma = \Lambda^{(0)}, \tag{2}$$

$$S = -\frac{1}{eT}\left(\frac{\Lambda^{(1)}}{\Lambda_{(0)}}\right), \tag{3}$$

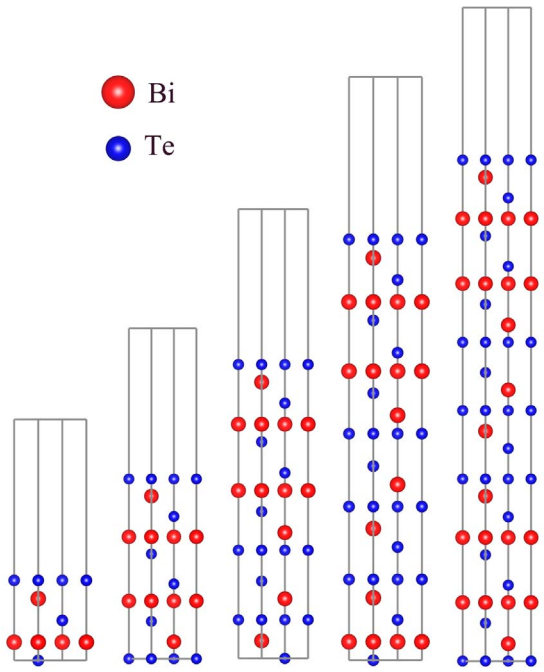

Figure 1 | Simulation models of the Bi_2Te_3 nanofilms with five different thicknesses: 1QL, 2QL, 3QL, 4QL and 5QL.

$$\kappa_e = \frac{1}{e^2T}\left\{\Lambda^{(2)} - \frac{\left[\Lambda^{(1)}\right]^2}{\Lambda^{(0)}}\right\}, \tag{4}$$

$$\Lambda^{(\alpha)} = \int d\varepsilon\left(-\frac{\partial f_0}{\partial \varepsilon}\right)(\varepsilon - E_F)^{\alpha}\Sigma(\varepsilon), \tag{5}$$

where e is the charge of the carriers, T is the temperature, E_F is the Fermi level, f_0 is the Fermi-Dirac distribution function, and $\sum(\varepsilon)$ is the transport distribution function and can be expressed as[31,35]

$$\sum(\varepsilon) = \frac{e^2}{N_{\mathbf{k}}\Omega}\sum_{\mathbf{k}}\mathbf{v}_{\mathbf{k}}\mathbf{v}_{\mathbf{k}}\tau_{\mathbf{k}}\delta(\varepsilon - \varepsilon(\mathbf{k})), \tag{6}$$

where $\mathbf{v}_{\mathbf{k}}$ is the group velocity of the carriers associated with wave vector $\mathbf{k}$, $\tau_{\mathbf{k}}$ is the relaxation time, $N_{\mathbf{k}}$ is the number of the sampled $\mathbf{k}$ points in the Brillouin Zone (BZ), and Ω is the volume of unit cell. For a quasi-two-dimensional (2D) system, Ω should be substituted by the product of Γ and h, where Γ is the area of a 2D unit cell and h is the thicknesses of the quasi-2D system. As a result, for the quasi-2D system Eq. (6) can be expressed as

$$\sum(\varepsilon) = \frac{e^2}{N_{\mathbf{k}}\Gamma h}\sum_{\mathbf{k}}\mathbf{v}_{\mathbf{k}}\mathbf{v}_{\mathbf{k}}\tau_{\mathbf{k}}\delta(\varepsilon - \varepsilon(\mathbf{k})). \tag{7}$$

Because the current version of the BoltzTrap program[36] is restricted to analyze 3D materials, according to the discussion above we implemented the codes (modified from the BoltzTrap codes[36]) for quasi-2D systems to obtain the transport coefficients.

The relaxation time τ depends on the temperature, electronic energy and carrier concentration and generally is treated as a constant for convenience. Due to lack of available data for the relaxation time of Bi_2Te_3 nanofilms, we have adopted the bulk value as a reliable approximation by noting that the nanofilms possess similar covalent bonds with bulk Bi_2Te_3[23]. Similar treatments have been done for nanoscale systems such as Si nanowires[33], Bi_2Te_3 nanowires[37], Bi_2Te_3 nanofilms[23], and so on. For the relaxation time at 300 K, we used the value of 2.2×10^{-14} s, which T. J. Scheidemantel *et al*[32] have adopted to study the thermoelectric properties of bulk Bi_2Te_3 and obtained consistent results with the experimental data[38]. The temperature dependence of the relaxation time of bulk Be_2Te_3 has been summarized in Table 1[37]. The phonon thermal conductivity is another important parameter to determine the thermoelectric figure of merit. The previous theoretical study showed that phonon thermal conductivity of the perfect 1QL Bi_2Te_3 nanofilm decreases monotonically with temperature and exhibits a T^{-1} dependence[23,24], and this inverse temperature dependence has also been found in bulk Bi_2Te_3 both theoretically[39] and experimentally[40]. For the perfect Bi_2Te_3 nanofilms with a few QL, the inverse temperature dependence[24] $\frac{b}{T}$ will be adopted in our calculations, and the coefficient b was determined by the value of the phonon thermal conductivity of Bi_2Te_3 nanofilms at 300 K[24]. Previous results showed that the thermal conductivity of few-quintuple Bi_2Te_3 nanofilms could be significantly reduced by introducing structure defects such as nanopore[24]. In the following, we also investigated the thermoelectric figure of merit of nanoporous Bi_2Te_3 nanofilms with few quintuples by assuming the defects don't significantly influence the electronic structure. Since the molecular dynamics simulation showed the thermal conductivity of nanoporous nanofilms depends weakly on the temperature and film thickness, we adopted a constant value of 0.3 W/mK in our calculation[24].

Results and discussion

Band structure. The *ab initio* electronic band structures of Bi_2Te_3 bulk material and nanofilms with various thicknesses are shown in Fig. 2. The spin-orbit interaction was taken into account in the calculation, which was proved to be essential for calculating the electronic structures of Bi_2Te_3, and our results for bulk Bi_2Te_3 (Fig. 2(a)) are in good agreement with the data reported in previous work[41]. As shown in Figs. 2(b–f), band structures of the Bi_2Te_3 nanofilms are similar to each other except for the significant difference in band gap and energy spacing between adjacent bands. Firstly, the indirect band gap decreases with increasing the film thickness. For example, the

Table 1 | Temperature dependence of the relaxation time of the bulk Bi_2Te_3[37]

Parameter	Temperature Dependence	
Mobility μ	$\mu_e \approx T^{-2.0}$	$\mu_h \approx T^{-1.7}$
Effective mass m	$m_e \approx T^{0.12}$	$m_h \approx T^{0.17}$
Relaxation time τ	$\tau_e \approx T^{-1.88}$	$\tau_h \approx T^{-1.53}$

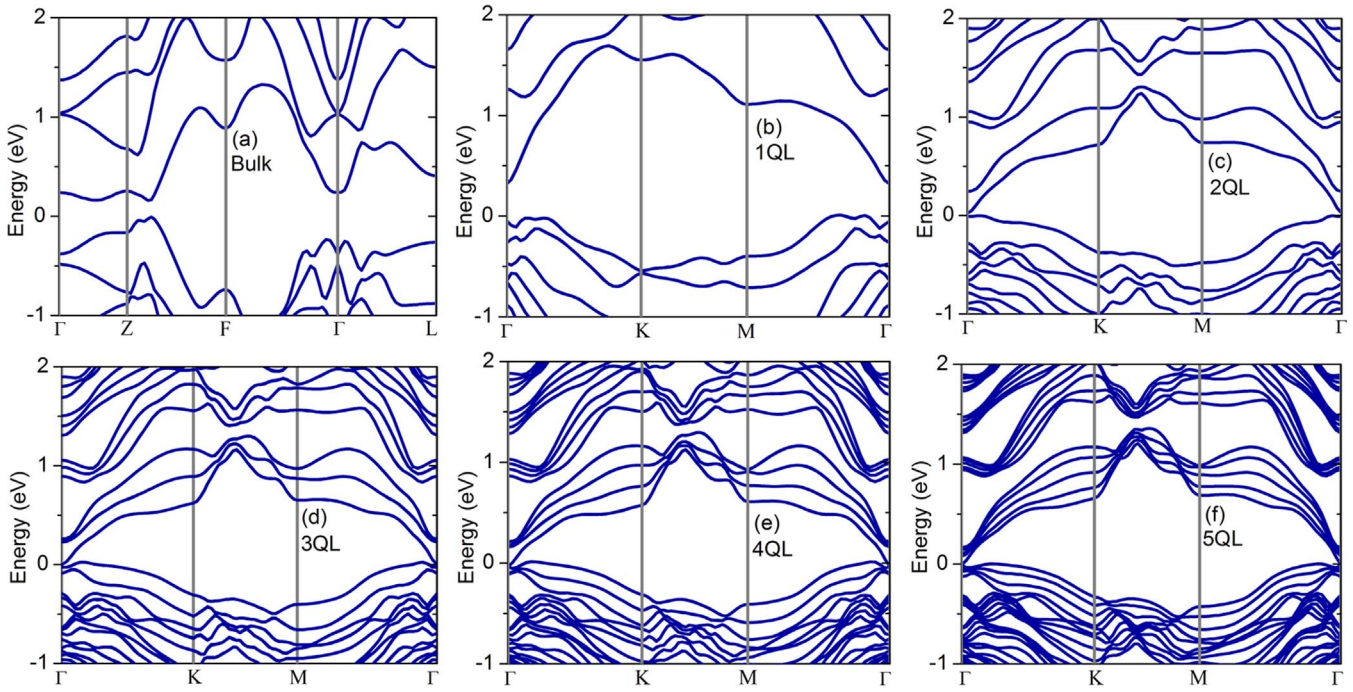

Figure 2 | Band structures of the bulk Bi_2Te_3 (a) and Bi_2Te_3 nanofilms with five different thicknesses: 1QL (b), 2QL (c), 3QL (d), 4QL (e), 5QL (f).

band gap is about 320 meV for 1QL film (Fig. 2(b)) and it disappears when the film thickness increases to 3QL (Fig. 2(d)). Secondly, the energy spacing between the adjacent bands decreases with increasing the number of QL. The reasons are that with the thickness increasing, the coupling between the top and bottom electronic states and the quantum confinement effect on the electrons in the nanofilm are weakened. It is also noteworthy to point out that the conduction bands of all five nanofilms are much more dispersive than the valence bands.

The density of states (DOS) for the Bi_2Te_3 nanofilms with various thicknesses is shown in Fig. 3. The DOS near the edge of the valence band has a sharper and larger peak than that near the edge of the conduction band due to flatter valence bands (as shown in Fig. 2). It can be observed from Fig. 3 that the total DOS for 1 QL Bi_2Te_3 nanofilm displays staircase-like behavior near the edges of conduction bands and valence bands, induced by the quantum confinement effect in quasi-2D systems. With the number of QL decreasing, the spacing between the peaks (singularity) of the DOS significantly increases, which is consistent with the change of the energy spacing between the adjacent bands.

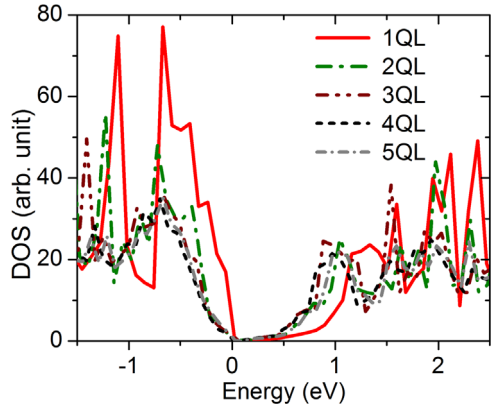

Figure 3 | Total density of states of the Bi_2Te_3 nanofilms with various thicknesses.

Transport properties. Based on the calculated electronic band structures, the thermoelectric transport coefficients of the few-quintuple Bi_2Te_3 nanofilms can be evaluated by the methods presented in Sec. II. It is well known that the standard density functional theory usually underestimates the band gaps of semiconductors. In order to achieve a better agreement with the experimental results, the band gaps of the nanofilms were adjusted to match the experimental data[42] by applying the so-called scissor operator in our calculations. Similar treatments have been widely adopted in previous publications[43,44].

Fig. 4 shows the calculated electrical conductivity, Seebeck coefficient, power factor and figure-of-merit of the perfect p-type Bi_2Te_3 films with different QL and p-type bulk Bi_2Te_3 as a function of carrier concentration at 300 K. As shown in Fig. 4(a), the electrical conductivity of all the p-type Bi_2Te_3 nanofilms increases with increasing carrier concentration. In contrast, the Seebeck coefficient decreases with increasing carrier concentration and in general the Seebeck coefficient for the thinner nanofilm is larger than that for the thicker nanofilm at the same carrier concentration (Fig. 4(b)). This can be explained by the following discussion. Taking into account that Maxwell-Boltzmann approximation is justified in the region of $E_F - E_V \gg k_BT$, S can be expressed as a function of n:

$$S = -\frac{k_B}{e}\ln\left(\frac{n}{N_V}\right) + \frac{k_B}{e}A_V, \tag{8}$$

where N_V is the effective density of states at the edge of the highest valence band and A_V represents a scattering factor of the semiconductor[8]. N_V can be expressed as

$$N_V = \int_{-\infty}^{E_V} g_V(\varepsilon)\exp[-(E_V-\varepsilon)/k_BT]d\varepsilon, \tag{9}$$

where $g_V(\varepsilon)$ is the density of states. Eq. (8) directly reveals that the magnitude of S decreases with increasing n, as shown in Fig. 4(b). In addition, with the number of QL decreasing, the DOS near the edge of the valence band increases due to the quantum confinement effect (Fig. 3), leading to an increase of N_V and hence an enhancement of S. It is worth noting that S of 1QL Bi_2Te_3 nanofilm is significantly larger than those of other nanofilms, which results from the significantly

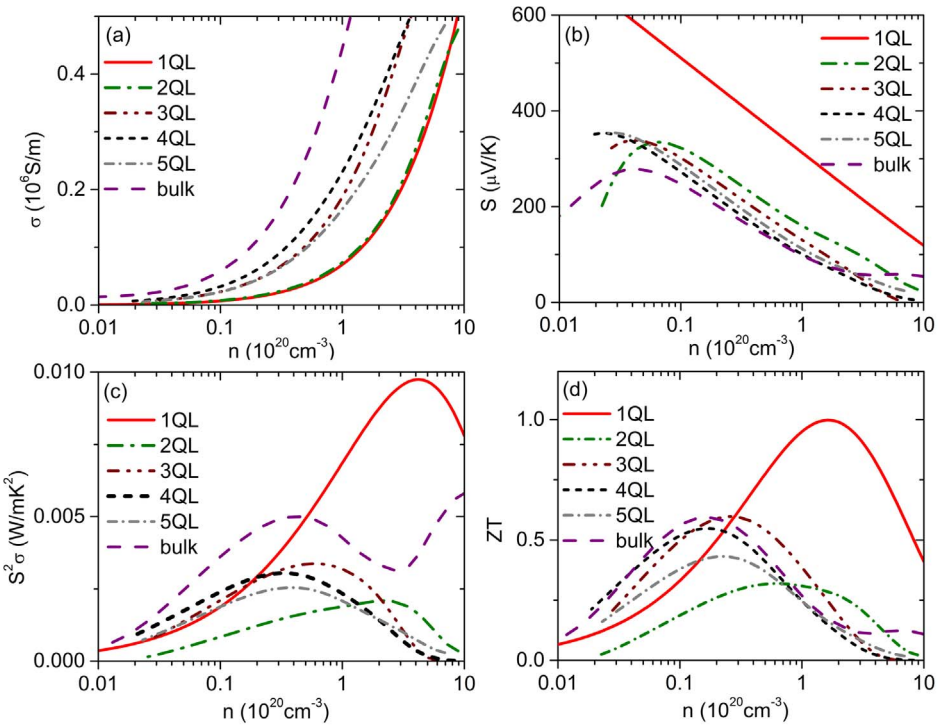

Figure 4 | Electrical conductivity (a), Seebeck coefficient (b), power factor (c) and figure of merit (d) of p-type perfect Bi_2Te_3 nanofilms with different thicknesses and p-type bulk Bi_2Te_3 as a function of carrier concentration at 300 K.

enhanced DOS near the edge of the valence band induced by the strong coupling between the top and bottom electronic states and the quantum confinement effect. The electrical conductivity σ increases with increasing carrier concentration n, whereas the Seebeck coefficient S decreases, therefore, there is an optimized carrier concentration, n_{opt}, at which the power factor is maximized (as shown in Fig. 4(c)). The n_{opt} to obtain the maximum power factor for Bi_2Te_3 nanofilms with various QL occurs in the range from 0.3×10^{20} cm^{-3} to 5×10^{20} cm^{-3}. In general, the n_{opt} increases with decreasing the number of QL. The n_{opt} can be derived as[8]

$$n_{opt} = N_V \exp(-2 + A_V). \quad (10)$$

Eq. (10) reveals that the n_{opt} for the power factor is proportional to N_V. With the number of QL decreasing, the DOS near the edge of the valence band increases, thus, N_V rises and hence n_{opt} increases (as shown in Fig. 4(c)). Figure 4(d) shows that the dependence of ZT on the carrier concentration is similar to that of the power factor, indicating that the carrier concentration is a key parameter to adjust the thermoelectric performance of the few-quintuple films. The n_{opt} to obtain the highest ZT value is in the range from 0.1×10^{20} cm^{-3} to 1.5×10^{20} cm^{-3}. The perfect 1QL film has the largest ZT value of 1.0 at an n_{opt} of 1.5×10^{20} cm^{-3}. The n_{opt} for the ZT is different from that for the power factor because of the effect of the electronic thermal conductivity that is related to the carrier concentration. We have calculated the thermoelectric transport properties of bulk Bi_2Te_3 by using the value of 2.2×10^{-14} s at 300 K[32] for the relaxation time and the value of 1.5 W/mK at 300 K[32] for the phonon thermal conductivity. Our calculated results are in excellent agreement with the previous theoretical[32] and experimental data[38]. It can be seen from Fig. 4 that the electrical conductivity of bulk Bi_2Te_3 is larger while the seebeck coefficient is smaller in most range of carrier concentrations, as compared with those of Bi_2Te_3 nanofilms at a fixed carrier concentration. The optimized ZT value of bulk Bi_2Te_3 is about 0.6, which is smaller than that of 1QL Bi_2Te_3 nanofilm (Fig. 4(d)).

Fig. 5 shows the calculated electrical conductivity, Seebeck coefficient, power factor and figure of merit of the p-type perfect 1QL Bi_2Te_3 nanofilm as a function of carrier concentration at different temperatures. As shown in Fig. 5(a), at a fixed carrier concentration the electrical conductivity decreases with increasing temperature, mainly because the scattering rate of the carriers increases and the relaxation time decreases with increasing temperature (as shown in Table 1). In contrast, the S slightly increases with increasing the temperature at a fixed carrier concentration, as shown in Fig. 5(b). This is mainly because when the temperature rises, the term, $\exp[-(E_V - \varepsilon)/k_BT]$ with $\varepsilon < E_V$, in Eq. (9) increases and then it leads to an increasing N_V. Due to the reduction of σ, the power factor decreases with increasing temperature and the n_{opt} to obtain the maximum power factor shifts to a larger value (Fig. 5(c)). Fig. 5(d) shows that the dependence of ZT on the temperature is reversed as compared with that of the power factor. Although the power factor decreases with raising temperature, ZT value increases because both phonon and electron thermal conductivity decrease. The peak values of ZT for the p-type perfect 1QL Bi_2Te_3 film are 1.0 and 1.9 at 300 K and 800 K, respectively.

Figs. 6(a) and 6(b) summarize the dependence of the optimized ZT (at n_{opt}) of the p-type perfect and nanoporous Bi_2Te_3 nanofilms with various QL on temperature, respectively. As shown in Fig. 6(a), for all of the perfect nanofilms, their optimized ZT values increase with increasing temperature and 1QL nanofilm has the highest optimized ZT value in the entire temperature range as compared with other nanofilms. The temperature dependence of optimized ZT value has also been found in the previous study of thermoelectric properties of 1QL Bi_2Te_3 nanofilm[23]. For the nanofilms with a thickness larger than 1QL, their ZT values are close to each other because they possess approximately similar DOS near the edge of the valence band. Previous results showed that the perfect nanofilms have high thermal conductivity, e.g. 1.65 W/mK for perfect 1QL nanofilm at 300 K[24], which limits further improvement of ZT. Fortunately, the molecular dynamics simulations showed that the phonon thermal conductivity can be significantly reduced by introducing structure defects such as nanopore[24]. Considering the fact that phonon thermal conductivity can be significantly reduced by introducing defects without significantly sacrificing the thermoelectric power factor $S^2\sigma$[45], which has

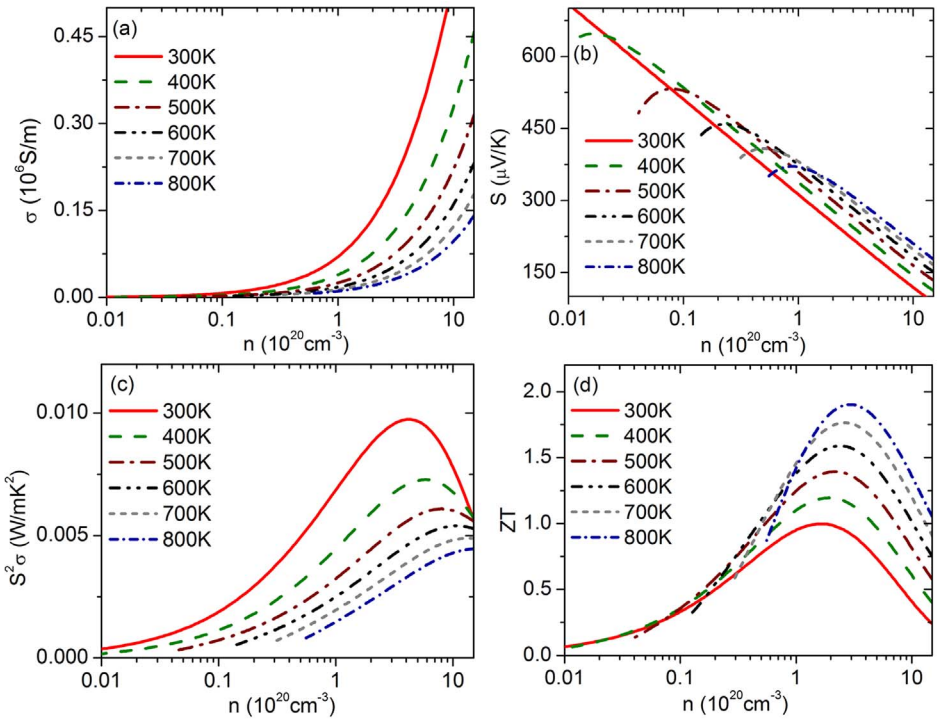

Figure 5 | Electrical conductivity (a), Seebeck coefficient (b), power factor (c) and figure of merit (d) of p-type perfect 1QL Bi_2Te_3 nanofilm as a function of carrier concentration at different temperatures.

been seen as a main strategy[2] to enhance the thermoelectric properties of materials and has been confirmed by a lot of experimental works[2,45,46], we give the calculated results of thermoelectric properties of nanoporous Bi_2Te_3 nanofilms by assuming that introduction of nanopores don't influence the electronic structure and power factor of nanofilms. Due to the reduction of phonon thermal conductivity, the p-type Bi_2Te_3 nanofilms with nanopore defects exhibit a significantly improved ZT value as compared with the perfect nanofilms. Particularly, the 1QL nanoporous Bi_2Te_3 nanofilms can achieve an optimized ZT value of 2.65 at room temperature, as shown in Fig. 6(b). The temperature dependence of the optimized ZT values of the p-type Bi_2Te_3 nanofilms with nanopore defects becomes complicated in comparison to that of the perfect nanofilms. This can be explained by the following discussions. By using the Wiedemann–Franz law: $\kappa_e = L\sigma T$, the ZT may be written as follows:[4]

$$ZT = \frac{S^2/L}{1+\frac{\kappa_l}{\kappa_e}}. \qquad (11)$$

For perfect Bi_2Te_3 nanofilms, the phonon dominates thermal transport ($\kappa_l \gg \kappa_e$), and ZT increases with temperature mainly due to that κ_l decreases with temperature. For nanoporous Bi_2Te_3 nanofilms, κ_l remains constant over the entire temperature range and ZT depends on temperature through S and κ_e according to Eq. (11). In this case, the values of κ_l and κ_e at optimized carrier concentration are comparable to each other. The temperature dependence of the optimized ZT values of nanoporous Bi_2Te_3 nanofilms is less prominent than that of perfect nanofilms, and several factors including S and κ_e as well as its magnitude relative to κ_l come into effect. We hope that these predictions could provide a clue for experimental researchers to optimize the thermoelectric performance of Bi_2Te_3 nanofilms.

Conclusions

In summary, we have employed a combination of first-principles electronic structure and Boltzmann transport calculations to predict the thermoelectric transport properties of few-quintuple Bi_2Te_3 nanofilms. Our results show that p-type Bi_2Te_3 nanofilms could be good candidates for thermoelectric nanomaterials, provided that the phonon thermal conductivity can be decreased by introducing structure defects without significantly sacrificing the thermoelectric power factor, and p-type 1QL nanofilm with nanopore defects can

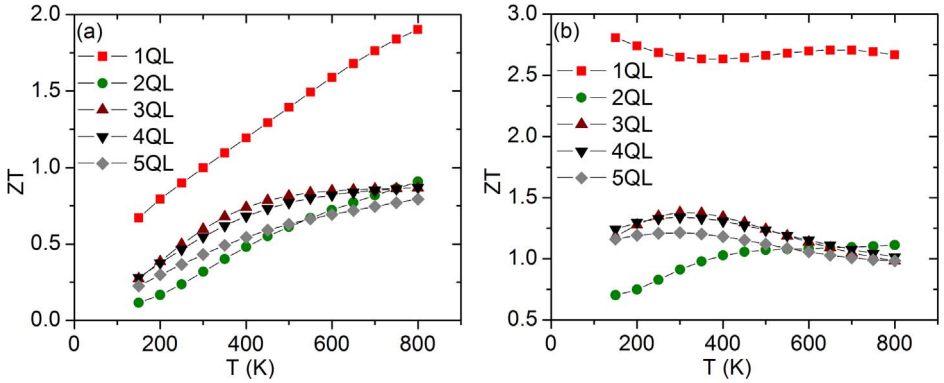

Figure 6 | Optimized figure of merit of the p-type perfect (a) and nanoporous (b) Bi_2Te_3 nanofilms with various quintuples as a function of temperature.

achieve an upper-limit *ZT* value of 2.65 at room temperature. It was found out that the p-type 1QL Bi_2Te_3 nanofilm as compared with other nanofilms has the highest *ZT* value, which is mainly attributed to the significantly enhanced density of states resulting from the strong coupling between the top and bottom electronic states and the quantum confinement effect. The dependence of thermoelectric transport properties on doping level and temperature was investigated in detail, which provides guidance for future experiments to optimize *ZT* value of p-type Bi_2Te_3 nanofilms with few quintuple layers. The type of calculation reported in this work represents a valuable investigation tool to study the thermoelectric properties of quasi-2D nanomaterials.

1. Biswas, K. *et al.* High-performance bulk thermoelectrics with all-scale hierarchical architectures. *Nature* **489**, 414–418 (2012).
2. Dresselhaus, M. S. *et al.* New Directions for Low-Dimensional Thermoelectric Materials. *Adv. Mater.* **19**, 1043–1053 (2007).
3. Liang, W. *et al.* Field-effect modulation of Seebeck coefficient in single PbSe nanowires. *Nano Lett.* **9**, 1689–1693 (2009).
4. Snyder, G. J. & Toberer, E. S. Complex thermoelectric materials. *Nat. Mater.* **7**, 105–114 (2008).
5. Pernstich, K., Rössner, B. & Batlogg, B. Field-effect-modulated Seebeck coefficient in organic semiconductors. *Nat. Mater.* **7**, 321–325 (2008).
6. Balandin, A. & Wang, K. L. Significant decrease of the lattice thermal conductivity due to phonon confinement in a free-standing semiconductor quantum well. *Phys. Rev. B* **58**, 1544–1549 (1998).
7. Hochbaum, A. I. *et al.* Enhanced thermoelectric performance of rough silicon nanowires. *Nature* **451**, 163–167 (2008).
8. Zhou, G., Li, L. & Li, G. Semimetal to semiconductor transition and thermoelectric properties of bismuth nanotubes. *J. Appl. Phys.* **109**, 114311 (2011).
9. Zhou, G., Li, L. & Li, G. Enhancement of thermoelectric figure of merit in bismuth nanotubes. *Appl. Phys. Lett.* **97**, 023112–023114 (2010).
10. Tavkhelidze, A. Large enhancement of the thermoelectric figure of merit in a ridged quantum well. *Nanotechnology* **20**, 405401–405406 (2009).
11. Zhao, Y., Dyck, J. S., Hernandez, B. M. & Burda, C. Enhancing thermoelectric performance of ternary nanocrystals through adjusting carrier concentration. *J. Am. Chem. Soc.* **132**, 4982–4983 (2010).
12. Yu, B. *et al.* Enhancement of thermoelectric properties by modulation-doping in silicon germanium alloy nanocomposites. *Nano Lett.* **12**, 2077–2082 (2012).
13. Poudel, B. *et al.* High-thermoelectric performance of nanostructured bismuth antimony telluride bulk alloys. *Science* **320**, 634–638 (2008).
14. Venkatasubramanian, R., Siivola, E., Colpitts, T. & O'quinn, B. Thin-film thermoelectric devices with high room-temperature figures of merit. *Nature* **413**, 597–602 (2001).
15. Fan, S. *et al.* p-type $Bi_{0.4}Sb_{1.6}Te_3$ nanocomposites with enhanced figure of merit. *Appl. Phys. Lett.* **96**, 182104–182106 (2010).
16. Sun, Z., Liufu, S., Chen, X. & Chen, L. Tellurization: An Alternative Strategy to Construct Thermoelectric Bi_2Te_3 Films. *J. Phys. Chem. C* **115**, 16167–16171 (2011).
17. Hasan, M. Z. & Kane, C. L. Colloquium: topological insulators. *Rev. Mod. Phys.* **82**, 3045–3067 (2010).
18. Zahid, F. & Lake, R. Thermoelectric properties of Bi_2Te_3 atomic quintuple thin films. *Appl. Phys. Lett.* **97**, 212102 (2010).
19. Li, X., Ren, H. & Luo, Y. Electronic structure of bismuth telluride quasi-two-dimensional crystal: A first principles study. *Appl. Phys. Lett.* **98**, 083113–083115 (2011).
20. Goyal, V., Teweldebrhan, D. & Balandin, A. Mechanically-exfoliated stacks of thin films of Bi_2Te_3 topological insulators with enhanced thermoelectric performance. *Appl. Phys. Lett.* **97**, 133117–133119 (2010).
21. Sung, J. H. *et al.* Atomic Layer-by-Layer Thermoelectric Conversion in Topological Insulator Bismuth/Antimony Tellurides. *Nano Lett.* **14**, 4030–4035 (2014).
22. Ghaemi, P., Mong, R. S. & Moore, J. E. In-Plane Transport and Enhanced Thermoelectric Performance in Thin Films of the Topological Insulators Bi_2Te_3 and Bi_2Se_3. *Phys. Rev. Lett.* **105**, 166603–166606 (2010).
23. Zhang, J. *et al.* Enhanced thermoelectric performance of a quintuple layer of Bi_2Te_3. *J. Appl. Phys.* **116**, 023706 (2014).
24. Qiu, B. & Ruan, X. Thermal conductivity prediction and analysis of few-quintuple Bi_2Te_3 thin films: A molecular dynamics study. *Appl. Phys. Lett.* **97**, 183107–183109 (2010).
25. Kresse, G. & Hafner, J. Ab initio molecular dynamics for liquid metals. *Phys. Rev. B* **47**, 558-561 (1993).
26. Kresse, G. & Furthmüller, J. Efficiency of ab-initio total energy calculations for metals and semiconductors using a plane-wave basis set. *Comput. Mater. Sci.* **6**, 15–50 (1996).
27. Kresse, G. & Furthmüller, J. Efficient iterative schemes for ab initio total-energy calculations using a plane-wave basis set. *Phys. Rev. B* **54**, 11169–11186 (1996).
28. Perdew, J. P. *et al.* Atoms, molecules, solids, and surfaces: Applications of the generalized gradient approximation for exchange and correlation. *Phys. Rev. B* **46**, 6671–6687 (1992).
29. Perdew, J. P. & Wang, Y. Pair-distribution function and its coupling-constant average for the spin-polarized electron gas. *Phys. Rev. B* **46**, 12947–12954 (1992).
30. Nakajima, S. The crystal structure of $Bi_2Te_{3-x}Se_x$. *J. Phys. Chem. Solids* **24**, 479–485 (1963).
31. Mahan, G. & Sofo, J. The best thermoelectric. *Proc. Natl. Acad. Sci. U.S.A.* **93**, 7436–7439 (1996).
32. Scheidemantel, T., Ambrosch-Draxl, C., Thonhauser, T., Badding, J. & Sofo, J. Transport coefficients from first-principles calculations. *Phys. Rev. B* **68**, 125210 (2003).
33. Vo, T. T., Williamson, A. J., Lordi, V. & Galli, G. Atomistic design of thermoelectric properties of silicon nanowires. *Nano Lett.* **8**, 1111–1114 (2008).
34. Ashcroft, N. W. & Mermin, N. D. *Solid State Physics* (Holt, Reinhart & Winston, Philadelphia, 1976).
35. Zhang, L., Du, M.-H. & Singh, D. J. Zintl-phase compounds with $SnSb_4$ tetrahedral anions: Electronic structure and thermoelectric properties. *Phys. Rev. B* **81**, 075117–075124 (2010).
36. Madsen, G. K. & Singh, D. J. BoltzTraP. A code for calculating band-structure dependent quantities. *Comput. Phys. Commun.* **175**, 67–71 (2006).
37. Bejenari, I. & Kantser, V. Thermoelectric properties of bismuth telluride nanowires in the constant relaxation-time approximation. *Phys. Rev. B* **78**, 115322–115333 (2008).
38. Goldsmid, H. J. *Thermoelectric Refrigeration* (Plenum, New York,1964).
39. Qiu, B. & Ruan, X. Molecular dynamics simulations of lattice thermal conductivity of bismuth telluride using two-body interatomic potentials. *Phys. Rev. B* **80**, 165203 (2009).
40. Satterthwaite, C. & Ure Jr, R. Electrical and thermal properties of Bi_2Te_3. *Phys. Rev.* **108**, 1164 (1957).
41. Mishra, S., Satpathy, S. & Jepsen, O. Electronic structure and thermoelectric properties of bismuth telluride and bismuth selenide. *J. Phys.: Condens. Matter* **9**, 461–470 (1997).
42. Li, Y.-Y. *et al.* Intrinsic topological insulator Bi_2Te_3 thin films on Si and their thickness limit. *Adv. Mater.* **22**, 4002–4007 (2010).
43. Xi, L. *et al.* Chemical bonding, conductive network, and thermoelectric performance of the ternary semiconductors Cu_2SnX_3 (X = Se, S) from first principles. *Phys. Rev. B* **86**, 155201 (2012).
44. Zou, D., Xie, S., Liu, Y., Lin, J. & Li, J. Electronic structures and thermoelectric properties of layered BiCuOCh oxychalcogenides (Ch = S, Se and Te): first-principles calculations. *J. Mater. Chem. A* **1**, 8888–8896 (2013).
45. Tang, J. *et al.* Holey silicon as an efficient thermoelectric material. *Nano Lett.* **10**, 4279–4283 (2010).
46. Xie, W. *et al.* Identifying the specific nanostructures responsible for the high thermoelectric performance of $(Bi, Sb)_2Te_3$ nanocomposites. *Nano Lett.* **10**, 3283–3289 (2010).

Acknowledgments

This work was supported by China Postdoctoral Science Foundation (Grant No. 2012M520236) and National Natural Science Foundation of China (Grant Nos. 21273124 and 21290190). Computational resources were provided by Tsinghua National Laboratory for Information Science and Technology of China.

Author contributions

G.Z. performed the calculations and modified the code. G.Z. and D.W. analyzed the data and discussed the results. All the authors reviewed the manuscript.

Additional information

Competing financial interests: The authors declare no competing financial interests.

How to cite this article: Zhou, G. & Wang, D. Few-quintuple Bi_2Te_3 nanofilms as potential thermoelectric materials. *Sci. Rep.* **5**, 8099; DOI:10.1038/srep08099 (2015).

This work is licensed under a Creative Commons Attribution-NonCommercial-NoDerivs 4.0 International License. The images or other third party material in this article are included in the article's Creative Commons license, unless indicated otherwise in the credit line; if the material is not included under the Creative Commons license, users will need to obtain permission from the license holder in order to reproduce the material. To view a copy of this license, visit http://creativecommons.org/licenses/by-nc-nd/4.0/